

24 average resistance for *P. aeruginosa* was 135.4 ± 25.04 G Ω , while MRSA had an average of
25 173.4 ± 16.28 G Ω . Using KPFM, the surface potential of MRSA shifted from -0.304 V to 0.153 V
26 and from -0.280 V to 0.172 V for *P. aeruginosa* on gold versus stainless steel substrates,
27 respectively. In an attempt to identify a potential charge carrier, peptidoglycan was also measured
28 with the ResiScope module and shown to have a resistance of 105 G Ω .

29 Keywords: Resiscope; bacteria; conductive AFM; nanoscale imaging; kelvin probe force
30 microscopy

31

32 **1. Introduction**

33 The World Health Organization (WHO) has deemed antimicrobial resistance a cardinal
34 threat facing humanity [1]. A report from the Centre for Disease Control (CDC), published in 2015
35 underscores this threat, estimating that approximately one in every 100 individuals infected with
36 drug resistant microbes will perish from such an infection [2]. This has caused a great deal of
37 interest in the development of alternate preventative and treatment methods effective against
38 resistance species of pathogenic bacteria, such as *Pseudomonas aeruginosa* and Methicillin-
39 resistant *Staphylococcus aureus* (MRSA).

40 Not only do bacteria gain resistance due to the heavy and widespread use of antimicrobials
41 in medicine, cleaning products, soaps, and sanitizers [1], but specialized communities of bacteria
42 cells, known as biofilms, are associated with inherent antimicrobial resistance and recalcitrance to
43 removal. Biofilms can easily proliferate within the human body, especially at wound sites where
44 the protective epithelium is compromised. Any biofilm infection, if not cleared, can be life-
45 threatening. Biofilms are initialized when bacteria adhere to a surface and begin to accumulate and
46 produce an extracellular matrix, which enmeshes and protects these organisms, while increasing

47 their adhesion strength. While antimicrobials are effective at eliminating the outer layers of
48 bacteria near the surface of the biofilm, the bottom layer, which is tightly bound to the substrate
49 and protected by the surrounding biomass, can persist and continue to proliferate [3,4].

50 MRSA and *P. aeruginosa* are opportunistic pathogens that form biofilms and are
51 commonly associated with nosocomial infections [5]. *P. aeruginosa* is a Gram-negative, rod-
52 shaped bacterium that is highly proficient in forming biofilms. The ability of *P. aeruginosa* to
53 attach and form biofilms on a range of metallic and non-organics surfaces, has caused serious
54 issues in hospitals (e.g. catheter infections in immunocompromised individuals) [6]. *P. aeruginosa*
55 is also responsible for complications in the treatment of illnesses that affect the respiratory system,
56 such as pneumonia or cystic fibrosis. Once inside the lungs, *P. aeruginosa* excretes a “slime”
57 matrix composed of various biological components that can affect cilia movement and cause
58 inflammation within the lungs, thus causing breathing complications [6]. This biofilm forming
59 ability makes *P. aeruginosa* especially dangerous when mixed with other bacteria, as biofilms can
60 turn a surface that is non-ideal for bacterial attachment into a surface to which other bacteria, such
61 as MRSA, will preferentially bind [5]. A single microbe attaching to a surface, can initiate a chain
62 reaction, creating an environment and surface more prone to infection of additional foreign,
63 pathogenic species, such as other bacterial strains, fungi and viruses [7,8]. MRSA is Gram-positive
64 cocci that once attached to a surface, secretes adhesins and toxins, facilitating attachment, all while
65 damaging the surrounding human cells and tissue [9]. Therefore, these two organisms are
66 particularly threatening to human health and require unique strategies to prevent, manage, and treat
67 infection.

68 In terms of creating antibacterial treatments that target bacterial biofilms, electricity has
69 shown great potential in disrupting bacterial adherence. The utilization of electricity as an

70 antimicrobial therapy has been investigated not only because it can reduce bacterial attachment,
71 but it may also accelerate the wound healing process, serving two essential functions in wound
72 healing therapy [10-12]. Cathodic current across conductive surfaces can reduce attachment by up
73 to 80%, potentially leading to the complete detachment of adherent bacteria [10]. Furthermore,
74 alternating current in wound healing applications on guinea pigs, speeds healing times when
75 directly applied to incised regions on the skin [13]. Therefore, researchers have begun creating
76 devices that allow for the application of electricity to a wound site. For example, Park et al. created
77 a polyester material coated with small, alternating Zn and Ag dots placed in an array across the
78 surface. The difference in electrical potentials between the dots caused microcurrents to be
79 generated across the wound site, affecting bacterial migration [14]. This is based on the principle
80 that under the influence of an electrical current, the motility of bacteria, such as *P. aeruginosa* and
81 *Escherichia coli* is impaired or guided in a specific direction via electrotaxis [15]. Although the
82 electrical inhibition of bacterial attachment has been well documented, we do not fully understand
83 the electrical properties of bacteria and how this influences bacterial behavior.

84 New state-of-the-art methods are being applied to characterize the surfaces charges of
85 bacteria and the impact of current on bacteria. Among these, AFM is a nanoscale imaging
86 technique that measures the topography of a surface. It has tremendous advantages over other
87 nano-imaging techniques such as scanning electron microscopy, in that it does not require drastic
88 changes in the environment (e.g. changes in pressure or temperature) to successfully image a
89 sample [16]. ResiScope is a module for AFM, in the category of conductive AFM (CAFM) that
90 simultaneously measures the current and resistance of a sample [17]. Similarly, Kelvin probe force
91 microscopy (KPFM) is a conductive mode of AFM that simultaneously measures the contact
92 potential difference between the tip and the sample. This value is a measure of the surface potential

93 [18]. This method of simultaneous acquisition provides a tremendous advantage in relating the
94 electrical properties of a sample to its physical structure. In this study, we utilized AFM, KPFM
95 and the ResiScope to simultaneously acquire topography, surface potential, and current to measure
96 the electrical resistance and surface potential of single MRSA and *P. aeruginosa* cells. Our goal
97 was to develop a framework for measuring biological molecules using conductive atomic force
98 microscopy (AFM), measures that will help us to understand how electrical current impacts
99 pathogenic bacteria.

100

101 **2. Methods**

102 *2.1 Bacterial strains and culture conditions*

103 Strains of *Pseudomonas aeruginosa* and Methicillin-resistant *Staphylococcus aureus* (MRSA)
104 were obtained from Dr. Scott Weese and Joyce Rousseau of the Pathobiology Department at the
105 University of Guelph. Strains were streaked and cultured on 5% blood agar plates and grown at
106 37°C for 24 hours before use. Individual colonies were chosen and transferred into 6 mL of tryptic
107 soy broth (TSB) solution to culture at 37°C in a shake incubator rotated at 200 rpm for 24 hours.
108 One mL of the bacterial broth was then transferred to 1.5 mL microfuge containers and centrifuged
109 at 1000 $\times g$ for 5 minutes. The excess liquid was then decanted, and the remaining cells were
110 resuspended into 1 mL of deionized water. This rinsing processes was repeated twice.

111

112 *2.2 Sample preparation for AFM/KPFM/ResiScope imaging*

113 Gold covered stainless steel discs, stainless steel discs, and sputter-coated gold mica substrates
114 (~100 nm coating) were used in these experiments as conductive interfaces. Clean, gold and
115 stainless steel discs were sonicated for 1 minute in de-ionized water to remove excess waste from

116 the surface. Substrates were then rinsed with 1 mL of deionized water and left to dry for 4 hours.
117 Four-hundred μL of the resuspended, rinsed bacterial solution was placed onto the stainless steel
118 and the Au-coated mica, while 250 μL were deposited onto the gold discs (amount chosen to
119 maximize surface coverage for each sample). Substrates were then incubated at room temperature
120 for 20 minutes, allowing for bacterial attachment. This length of time produces highly dispersed
121 populations for single cell imaging on the atomic force microscope. The excess solution on the
122 substrates was then gently rinsed with 1 mL of deionized water using a micropipette. Substrates
123 were allowed to dry overnight before imaging.

124

125 *2.3 Preparation of Au-Coated mica*

126 Mica sheets were cut into approximately 1.8 x 1.8 cm squares using sharp scissors. Individual
127 sheets were cleaved to ensure a clean, flat surface with no flaking. Mica sheets were then sputter-
128 coated under vacuum with ~ 100 nm of gold. This thickness allows for high current application in
129 measurements without the degradation of the thin metal film.

130

131 *2.4 Imaging AFM/KPFM/Resiscope*

132 All AFM imaging was done on the Agilent 5500 series AFM. The ResiScope module from
133 Concept Scientific Instruments was used to make current and resistance measurements.

134 The conversion of resistance imaging units in Volts to Ohms is given by $R = 10^{(V+2)}$. All
135 ResiScope images were taken with a potential of 0.7 V applied to the conductive substrate.
136 Conductivity imaging was done using conductive PtIr-coated Si tips of 75 kHz, 2N/m and 225 nm
137 in length. KPFM measurements were taken using Mikromasch Pt coated cantilevers of 75 kHz,
138 2N/m and 240 nm. Measured Cells were chosen based upon the lack of surrounding, noticeable

139 contamination (e.g. EPS), as well as their total exposed circumference. Single cells were targeted
140 for measurement in this experiment, leaving roughly at least half of the total cell circumference
141 exposed.

142 *2.5 Raman Spectroscopy*

143 All Raman measurements were done on the Advantage series near-infrared Raman spectrometer
144 by DeltaNu. A wavelength of 785 nm was used to collect spectra. Three centrifuged, rinsed
145 quantities of MRSA and *P. aeruginosa* were combined and resuspended in deionized water to
146 ensure a high concentration of cells. Twenty μL of rinsed bacterial solution was then deposited
147 onto gold SERS substrates from Ocean Optics and left to dry for a period of three days. Purified
148 peptidoglycan samples from *Staphylococcus aureus* were bought from Sigma-Aldrich. A 4 mg/mL
149 solution of peptidoglycan was left to settle for 1 minute. Twenty-five μL of the separated and
150 suspended peptidoglycan sample was then pipetted onto the SERS substrate and left to dry for
151 three days.

152

153 **3. Results**

154 *3.1 Bacterial resistivity and potential measurements*

155 Gold and stainless steel substrates were chosen for their conductive properties and medical
156 relevance. Conductive measurements were made on uncolonized bare and gold-coated stainless
157 steel and on the same surfaces after *P. aeruginosa* and MRSA were allowed to adhere. Due to the
158 roughness of the stainless steel, along with its increased reactivity (versus gold), we were
159 unsuccessful in taking measurements on this surface using the ResiScope. However, we were able
160 to acquire CAFM images of MRSA and *P. aeruginosa* on gold-coated surfaces (Figure 1). Table
161 1 shows the average resistance for bacterial cells adhered to the surface. The average resistance

162 for *P. aeruginosa* was 135 ± 25 G Ω , while MRSA had an average of 173 ± 16 G Ω . The two values
163 were not significantly different from one another. However, we may see differences with a larger
164 sample size, as the average is based on resistance values from an average of four cells. These
165 measurements are in alignment with those obtained in another study that quantified the resistance
166 of *E. coli* cells suspended across two, conductive gold interdigitated fingers; results resistance
167 values were ~ 396 G Ω [19].

168 We also acquired KPFM measurements of MRSA and *P. aeruginosa* on stainless steel and
169 gold-coated substrates to gain a better understanding of the relationship between surface potential
170 and potential charge transfer (Figure 2, Table 1). Both of the bacterial cell surface potentials
171 switched from negative to positive between the gold and stainless steel substrates. MRSA had a
172 surface potential of -0.304 V for gold and 0.153 V for stainless steel, and *P. aeruginosa* -0.280 V
173 for gold and 0.172 V for stainless steel. A similar effect was reported by Birkenhauer et al., where
174 the surface potential of MRSA cells switched from positive on stainless steel to negative on gold.
175 This suggests that surface potential varies across bacterial strains and is influenced by the surface
176 to which the cells bind [5]. Finally, in an attempt to measure charge transfer, a 500 x 500 nm close-
177 up resistance image of *P. aeruginosa* on gold was acquired (Figure 3). KPFM close-ups emphasize
178 the difference in surface potential at the cell-gold interface.

179 180 3.2 The role of peptidoglycan in potential measures

181 We went on to investigate which bacterial substances might be involved in forming the
182 conductive path shown in Figure 1. In solution, bacteria are conductive due to the functions of
183 their ion channels. However, their outer membranes are largely composed of polysaccharides and
184 lipids, which are non-conductive. Based on the structural properties of the membranes in MRSA
185 and *P. aeruginosa*, the bulk of the electrical measurements would be made while in contact with

186 the outer peptidoglycan layer. Therefore, we dried a 4 mg/mL of peptidoglycan on gold coated
187 mica for 24 hours at 37°C to image the electrically conductive properties of peptidoglycan to
188 determine if its resistive properties correlate with images of bacteria taken earlier. We found
189 micrometer sized islands of peptidoglycan had formed, with a height of approximately 40 nm in
190 height (Figure 4). To confirm that the purified peptidoglycan was indeed peptidoglycan, Raman
191 spectroscopy was used, and the results were correlated with scans of *P. aeruginosa* and MRSA
192 that show it is present in both samples (Figure 5). The peak at $\sim 730 \text{ nm}^{-1}$ is attributed to the
193 stretching of the glycosidic rings in the NAG and NAM molecules present in the peptidoglycan
194 layer surrounding the cells [19-20]. Relative intensity measures show a smaller peak for *P.*
195 *aeruginosa*, most likely due to the thinner layer of peptidoglycan and its partial obstruction by
196 lipopolysaccharides. This confirms that the molecule being measured on the surface is in fact
197 peptidoglycan. CAFM measurements of peptidoglycan on the gold sputter coated mica show an
198 average resistance value of 9.021 V or 105 G Ω (Figure 6). This resistance value will change
199 depending of the thickness of the peptidoglycan sample.

200

201 **4. Discussions**

202 AFM, KPFM, and ResiScope are excellent tools for studying the electrical potential of
203 bacteria, as demonstrated by our results. However, the conditions must be carefully controlled to
204 ensure ideal measurement. Controlling the quality of a ResiScope image can be accomplished by
205 varying the force setpoint and the potential applied on the substrate. By increasing the setpoint and
206 increasing the tip force exerted upon the sample, increased contact improves the consistency of the
207 conductance measurements. However, if the force is raised too high, it can wear the conductive
208 coating off the tip. Another option to produce a better electrical signal is to increase the potential

209 applied to the substrate, thus raising the flow of current from the substrate to the tip. However,
210 raising the voltage too high can increase the reactivity between the tip and the sample, leading to
211 degradation of the thin metal. For these reasons, the choice of tip becomes critical [17]. Originally,
212 we used the same platinum (Pt) tips for CAFM and KPFM. However, the Pt tips eroded rapidly,
213 wearing away the metal coating. For these reasons, PtIr tips were used, which increased the signal
214 response by providing a more stable flow of electrons [21]. PtIr contact mode tips with a low spring
215 constant of 0.1 N/m are superior to Pt tips, but still generate a significant amount of noise. After
216 testing PtIr tips with a midrange spring constant of 3 N/m and 75 kHz, we found these were ideal
217 for our task. The higher spring constant allowed for more consistent contact between the tip and
218 the surface. This combination gave the best and most consistent measurements for both biological
219 and test samples. Our experiences underscore the importance of carefully selecting best settings
220 and tips for CAFM analysis; we found that until a method is established for a particular sample
221 type, this is likely to be a trial and error process. Our work establishes a set a parameters that can
222 be used as a starting point for subsequent studies of a similar nature.

223 As for CAFM, we found that there are a variety of parameters that influence the success of
224 ResiScope analysis. The version of ResiScope currently used by our laboratory is limited to contact
225 mode. Contact mode, especially when used for inorganic samples, allows for better electrical
226 contact between the tip and the substrate, which leads to more stable measurements. However,
227 there are some shortcomings to using contact mode for these studies. First, it can easily dislodge a
228 sample from the surface if it is weakly bound. Second, the high friction force of the cantilever
229 pressing onto the metallic surface quickly erodes the thin film of conductive material deposited
230 onto the Si tips [16]. There is a potential for combining KPFM and ResiScope images to study
231 charge transfer, as a result of differences in the localized potential between the cell and the

232 substrate. Our results give a reasonable starting point for such studies, but additional optimization
233 is necessary to improve image quality for our application.

234 Our results and experiences demonstrate that there are a variety of options for enhancing
235 and optimizing the measurement of bacterial electrical properties using CAFM. The experiments
236 in this study provide a framework for future analysis and highlight several pathways for four
237 ongoing research. For example, one direction would be to study bacteria in a more hydrated
238 environment, similar to their natural habitat. Although, electrical measurements cannot be made
239 in liquid, an environment humid enough to maintain the cells in a moist climate could restore the
240 function of bacterial ion channels, while being conducive to CAFM, thereby allowing for the
241 measurement of their charge transfer properties. Although multi-drug resistant strains of bacteria
242 are highly relevant to the end application of this project, measuring a known conductive bacterium,
243 such as *G. sulfurreducens*, may also help in the development and optimization CAFM techniques
244 to be later be applied to less conductive strains. Furthermore, strains of *G. sulfurreducens* form
245 conductive biofilms [22-23], offering the potential for charge transference and propagation to be
246 studied in these much larger structures.

247 As denoted earlier, MRSA and *P. aeruginosa* strains were initially chosen for electrical
248 measurement, because they are two common opportunist pathogens that readily cause wound
249 infection. Wound infections represent a prime area where electrical current could be
250 therapeutically applied as it may help to remove bacteria, while accelerating wound healing. In
251 addition to comparing potential conductive differences between Gram-positive and Gram-negative
252 bacteria, the motile nature of *P. aeruginosa* allows for the imaging and investigation of the
253 electrical properties of pili and flagella. We plan to investigate this area further in future studies
254 and to apply these techniques to the study of other interesting or relevant bacteria. For example,

255 CAFM has direct measurement capabilities that could potentially help to elucidate how *G.*
256 *sulfurreducens* pili exhibit metallic-like conductivity [24-25].

257 It is not entirely clear which component(s) of the bacteria studied here are responsible for
258 conducting the charge. If peptidoglycan is acting as the charge carrier, it is somewhat surprising
259 then that *P. aeruginosa* does not display a higher resistivity, as it is covered by an outer layer of
260 lipopolysaccharides. This suggests that an alternate conductive structure may be responsible for
261 conductance observed in this study. This is something that we could investigate in future studies,
262 as we have several parameters worked out for examining external bacterial structures using
263 ResiScope. For the measurement of peptidoglycan, we switched the substrate from gold-coated
264 stainless steel to gold sputter-coated mica, because the high surface roughness of the original
265 substrates could potentially have made it difficult to distinguish the peptidoglycan from the surface
266 itself. Additionally, we determined that the gold-sputtered mica represents a much cleaner sample
267 that is less easily contaminated prior to imaging. Although residual material is washed off the gold-
268 coated stainless steel, the high surface roughness will retain a certain degree of contaminants from
269 the environment that can obstruct electrical measurements. Conversely, the cleaved mica provides
270 a pristine surface, ensuring that the only thing being measured is the purified peptidoglycan
271 sample. Direct measurements of dried bacterial cells are seldom collected; most electrical
272 measurements of bacteria focus on the planktonic state or individual live cells in solution [26]. Our
273 work provides a framework for the future measurement of bacterial conductance in individual
274 bacterial cells.

275

276

277

278 **5. Conclusions**

279 Our study successfully establishes a novel methodology for the imaging and analysis of
280 the conductance of single bacterial cells from medically relevant bacteria, such as *P. aeruginosa*
281 and MRSA. Our method is adaptable and can be modified as necessary to study the conductance
282 of other bacterial species or biological substances. The average resistance values obtained in our
283 study are comparable to those obtained in a prior study of *E. coli*, helping to validate our technique.
284 Our work opens the door to further investigation of the electrical properties of pathogenic bacteria,
285 information that will be essential in developing electroceuticals. Such approaches would be a great
286 benefit for wound healing, as early studies suggest that the application of an electrical current can
287 help to eliminate potential pathogens, while accelerating wound healing. However, to optimize
288 such treatments, a better understanding of the localized electrical properties of adherent bacteria is
289 necessary. Our work helps to establish a “toolbox” for investigating the electrical properties of an
290 array of bacterial species.

291

292 **Acknowledgements**

293 Financial support for this research was provided by the Natural Sciences and Engineering
294 Council of Canada (Grant#400705) and the Ontario Ministry of Research and Innovation (Grant
295 #300142). The authors would like to thank Dr. Scott Weese and Ms Joyce Rousseau of the
296 Pathobiology Department of the University of Guelph for providing bacterial strains as clinical
297 samples from canine patients.

298

299

300

301 **References**

302

303 1) World Health Organization 2015 Worldwide country situation analysis: response to
304 antimicrobial resistance. Retrieved from
305 http://apps.who.int/iris/bitstream/10665/163468/1/9789241564946_eng.pdf?ua=1&ua=1

306

307 2) Centers for Disease Control and Prevention 2013 Antibiotic Resistance Threats in the United
308 States. U.S. Department of Health and Human Services:1600 Clifton Road Atlanta, GA 30329-
309 4027 USA

310

311 3) Neethirajan S and Clond M 2014 Medical Biofilms-Nanotechnology Approaches *J. Biomed.*
312 *Nanotechnology.* **10** 1-22

313

314 4) Donlan R M 2002 Biofilms: microbial life on surfaces *Emerg. Infect. Dis.* **8**(9) 881-890

315

316 5) Birkenhauer E and Neethirajan S 2014 Characterization of electrical surface properties of mono-
317 and co-cultures of *Pseudomonas aeruginosa* and methicillin-resistant *Staphylococcus aureus* using
318 Kelvin probe force microscopy *RSC Adv.* **4** 42432–42440

319

320 6) Rehm B 2008 *Pseudomonas*: model organism, pathogen, cell factory, Weinheim, Wiley-VCH

321

322 7) Bertesteanu S, Triaridis S, Stankovic M, Lazar V, Chifiriuc M C, Vlad M and Grigore R 2014
323 Polymicrobial wound infections: Pathophysiology and current therapeutic approaches *Int. J.*
324 *Pharm.* **463** 119–126

325

326 8) Harmsen M, Yang L, Pamp S J, and Tolker-Nielsen T 2010 An update on *Pseudomonas*
327 *aeruginosa* biofilm formation, tolerance, and dispersal *FEMS. Immunol. Med. Mic.* **59** 253–268

328

329 9) Ofek I 1994 Bacterial adhesion to animal cells and tissues, New York, Chapman & Hall

330 10) Hong H S, Jeong J, Shim S, Kang H, Kwon S, Ahn K and Yoon J 2008 Effect of Electric
331 Currents on Bacterial Detachment and Inactivation *Biotechnol. Bioeng.* **100** 379-386

332

333 11) Borden A J, Mei H C, Busscher H J 2005 Electric block current induced detachment from
334 surgical stainless steel and decreased viability of *Staphylococcus epidermidis* *Biomaterials.* **26**
335 6731-6735

336

337 12) Kerr A, Hodgkiess T, Cowling M J, Beveridge C M, Smith M J and Parr A C S 1998 A Novel
338 Technique to Prevent Bacterial Fouling, Using Imposed Surface Potential *J. App. Microbiol.* **85**
339 1067-1072

340

341 13) Mehmandoust F G, Torkaman G, Firoozabadi M and Talebi G 2007 Anodal and Cathodal
342 Pulsed Electrical Stimulation on Skin Wound Healing in Guinea Pigs *J. Rehabil. Res. Dev.* **44** 611-
343 618

344

- 345 14) Park S, Kim H, Makin I, Skiba J and Izadjoo M 2015 Measurement of Microelectric potentials
346 in a Bioelectrically-Active Wound Care Device in the Presence of Bacteria *J. Wound. Care.* **24**
347 23-33
348
- 349 15) Shi W, Lentz M J, Adler J 1996 Effect of the Surface Composition of Motile *Escherichia coli*
350 and motile *Salmonella* Species on the Direction of Galvanotaxis *J. Bacteriol.* **178** 1113-1119
351
- 352 16) Eaton P J and West P 2010 Atomic force microscopy. New York, Oxford University Press
353
- 354 17) Resiscope User Guide 2011 *R10A*. Plateau de Saclay, France: Concept Scientific Instruments
355
- 356 18) Melitz W, Shen J, Kummel A C and Lee S 2011 Kelvin probe force microscopy and its
357 application *Surf. Sci. Rep.* **66** 1–27
358
- 359 19) Lu Y, Chuang Y, Chen Y, Shu A, Hsu H, Chang H and Yew T 2008 Bacteria Detection
360 Utilizing Electrical Conductivity *Biosens. Bioelectron.* **23** 1856-1861
361
- 362 20) Jarvis R M, Brooker A and Goodacre R 2006 Surface-enhanced Raman scattering for the rapid
363 discrimination of bacteria *Faraday. Discuss. R. Soc. Chem.* **132** 281-292
364
- 365 21) Jamond N, Chretien P, Houze F, Lu L, Largeau L, Mauain O, Travers L, Harmand J C, Glas
366 F, Lefeuvre E, Tchernycheva M and Gogneau N 2016 Piezo-generator integrating a vertical array
367 of GaN nanowires *Nanotechnology.* **27** 325403-325412
368
- 369 22) Malvankar N S and Lovley D R 2014 Microbial nanowires for bioenergy applications *Curr.*
370 *Opin. Biotech.* **27** 88-95
371
- 372 23) Malvankar N S, Tuominen M T and Lovley D R 2012 Lack of cytochrome involvement in
373 long-range electron transport through conductive biofilms and nanowires of *Geobacter*
374 *sulfurreducens* *Energ. Environ. Sci.* **9** 8651-8659
375
- 376 24) Veazey J P, Reguera G and Tessmer S H 2011 Electronic properties of conductive pili of the
377 metal-reducing bacterium *Geobacter sulfurreducens* probed by scanning tunneling microscopy
378 *Phys. Rev. E.* **84** 060901-1-4
379
- 380 25) Reguera G and McCarthy K 2005 Extracellular Electron Transfer via Microbial Nanowires
381 *Nature.* **435** 1098-1101
382
- 383 26) Mansor M A, Ahmad M R 2015 Single Cell Electrical Characterization Techniques *Int. J. Mol.*
384 *Sci.* **16** 12686-12712
385
386
387
388
389
390

391 **Table 1.** Average resistance and surface potential values for *P. aeruginosa* and MRSA on gold
392 and stainless steel. Increased surface roughness and tip-sample interactions rendered ResiScope
393 unable to retrieve viable measurements of resistance for stainless steel.

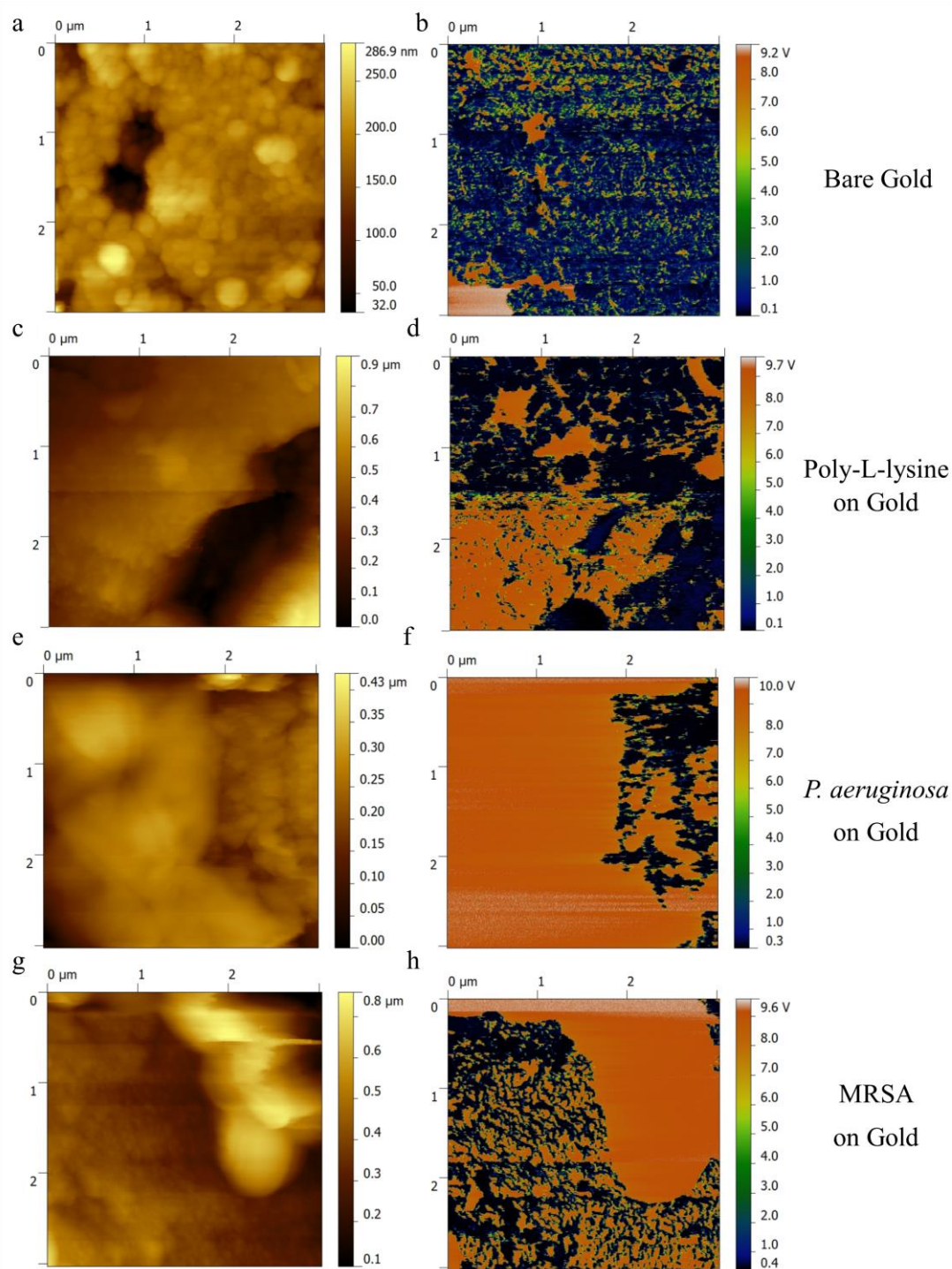
394
395

	Average Resistance: Au Substrate (GΩ)	Average Resistance: SS Substrate (GΩ)	Surface Potential on Gold Substrate (V)	Surface Potential on SS Substrate (V)
MRSA	173.4±16.28	---	-0.304±0.05	0.153±0.06
<i>P. aeruginosa</i>	135.4±25.04	---	-0.280±0.09	0.172±0.02

396
397
398
399
400
401
402
403
404
405
406
407
408
409
410
411
412
413
414
415
416
417
418
419
420
421
422
423
424

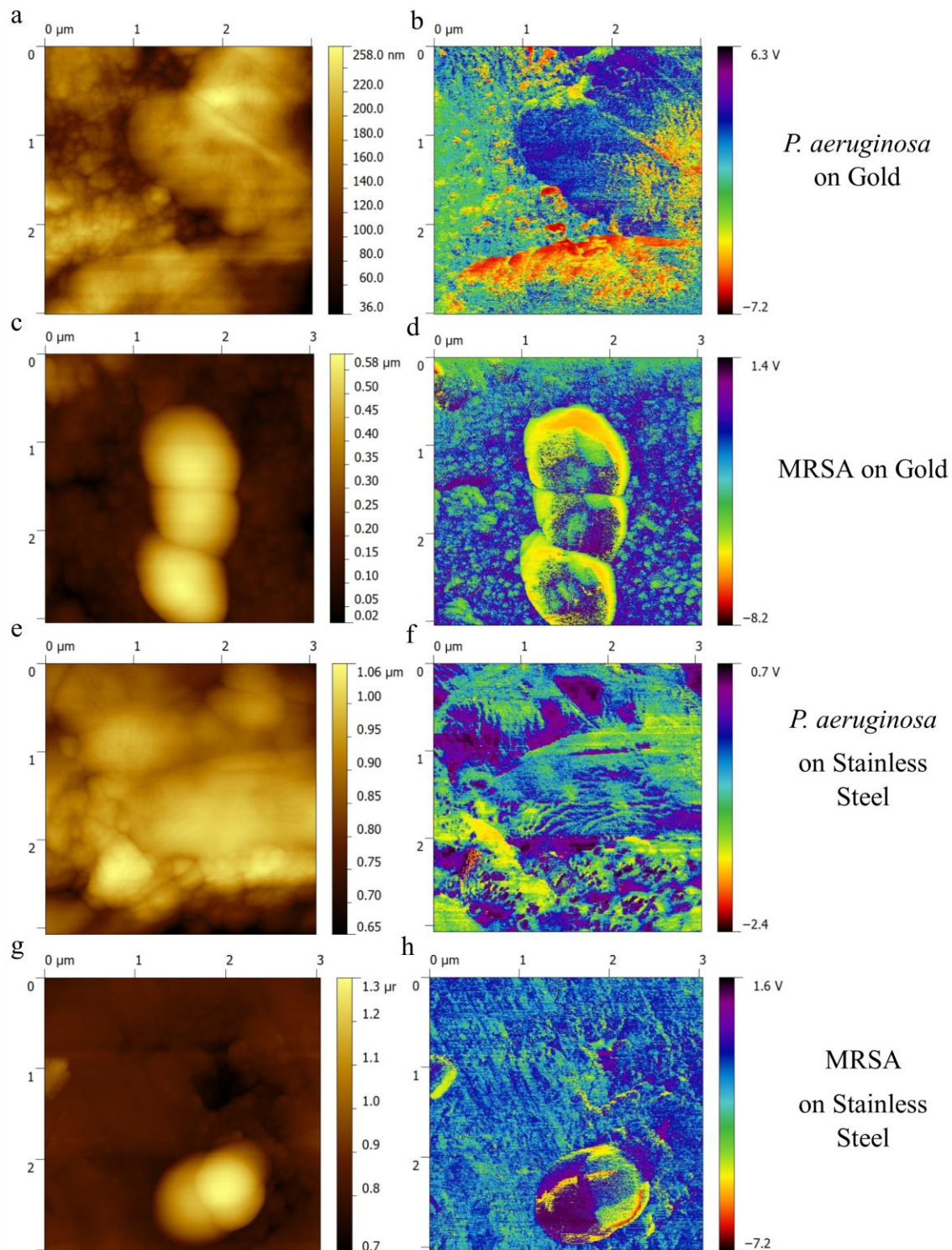
425
426

Figures



427
428 **Figure 1.** Topography and ResiScope resistance images of (a, b) bare gold, (c, d) gold-coated with
429 poly-L-lysine, (e, f) *P. aeruginosa* and (g, h) MRSA on gold. Application of poly-L-lysine causes
430 a slight increase in highly resistant artifacts on the surface of the gold, but the surface still remains
431 mostly highly conductive.

432



433

434 **Figure 2.** Topography and KPFM (surface potential) images of (a, b) *P. aeruginosa* on gold, (c,

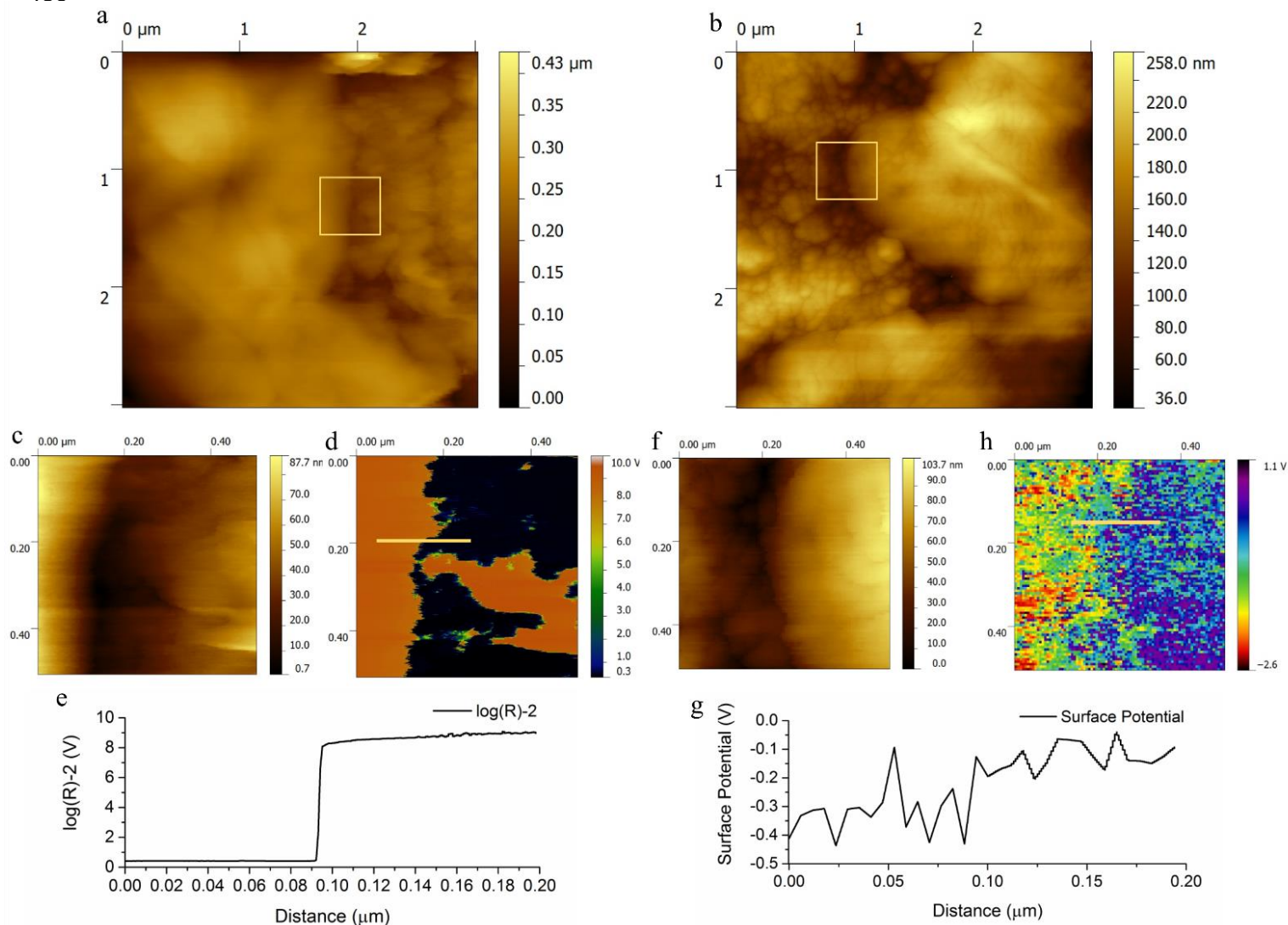
435 d) MRSA on gold, (e, f) *P. aeruginosa* on stainless steel and (g, h) MRSA on stainless steel.

436 Surface potential changes from negative for *P. aeruginosa* and MRSA on gold to positive on

437 stainless steel for both bacteria.

438

439



466

467

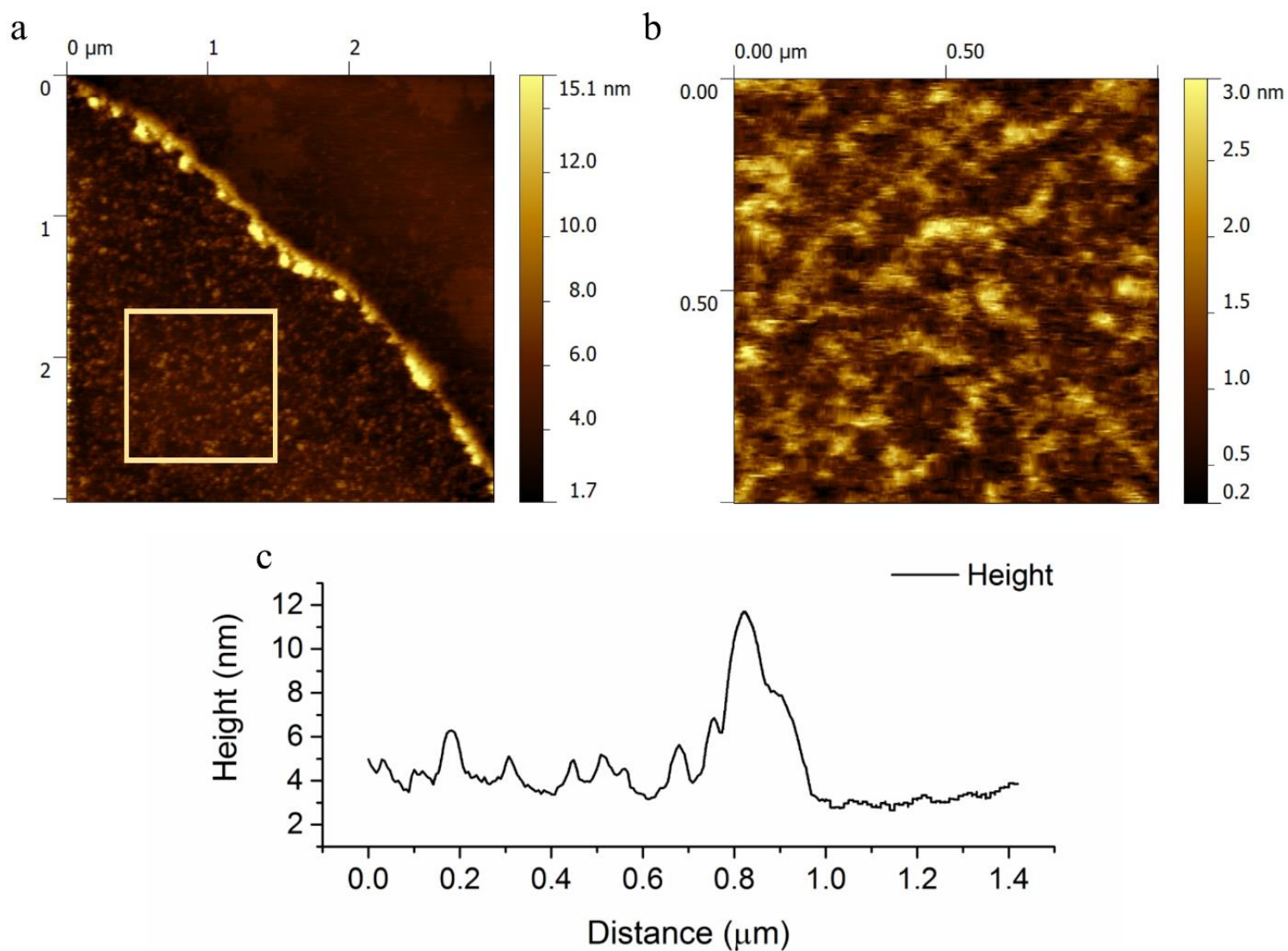
468 **Figure 3.** Original 3 x 3 μm zoomed out images of (a, b) *P. aeruginosa* on gold substrates. Zoomed
469 500 x 500 nm topographical scan (c) of *P. aeruginosa* membrane interface with gold substrate and
470 the corresponding resistance image (d). A cross section of the resistance image (e), showing a
471 steep change in resistance. Cropped 500 x 500 nm topographical scan (f) of *P. aeruginosa*
472 membrane interface with gold and the corresponding surface potential image (g). Line
473 measurement (h) of surface potential step from gold to bacterial surface.

474

475

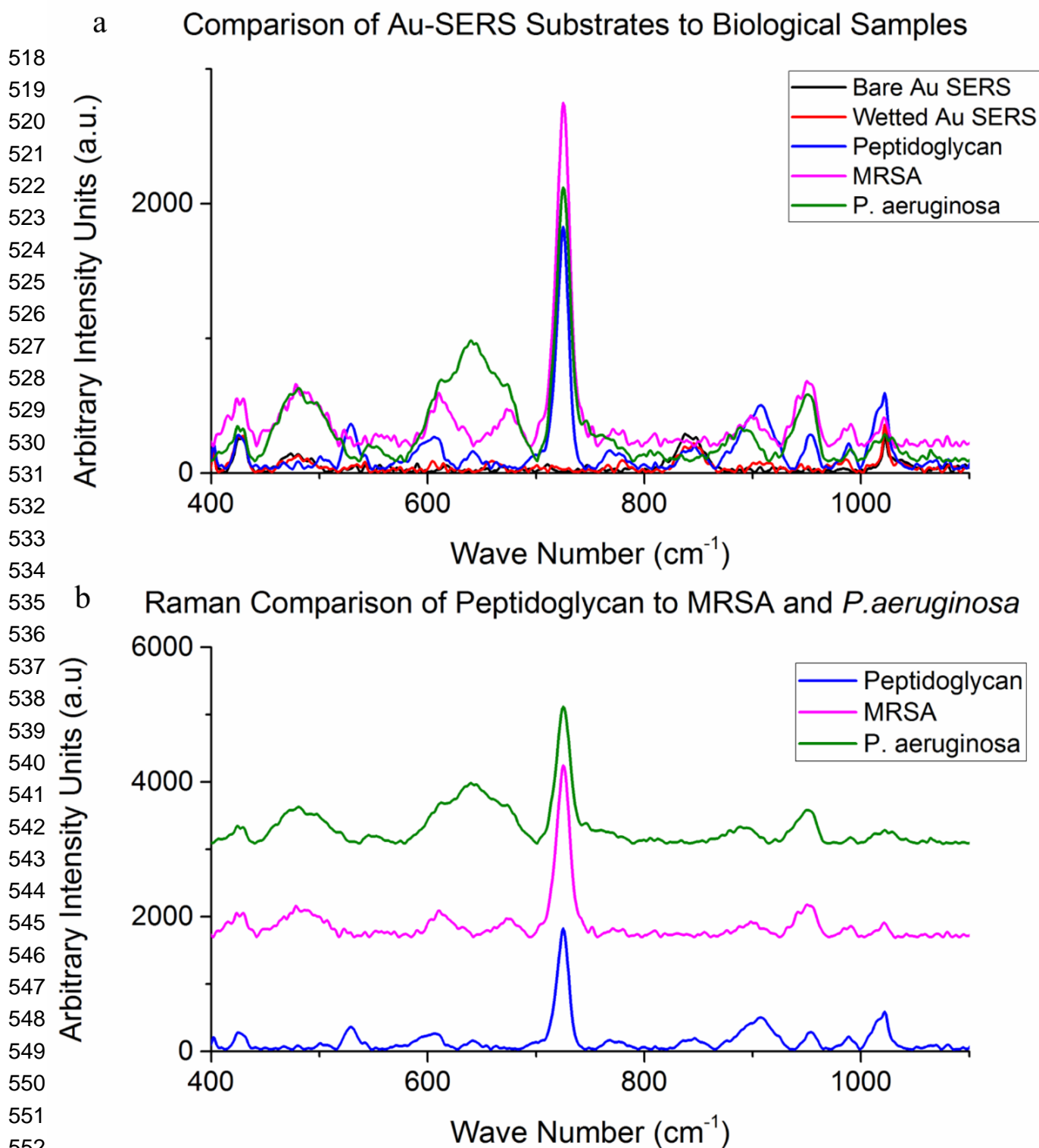
476

477

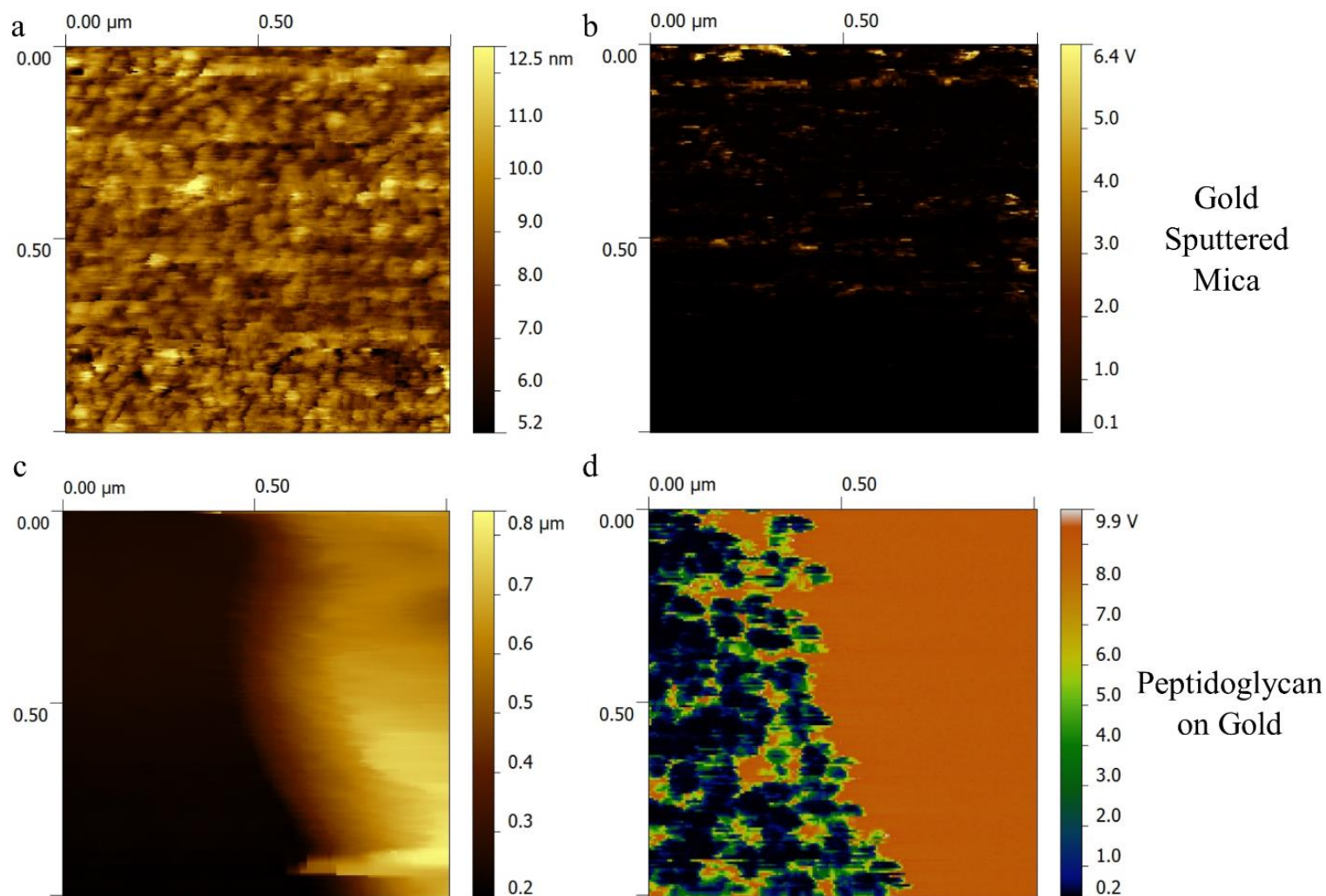


503
504 **Figure 4.** Topography images of peptidoglycan particle (a) on Au coated mica surface and (b)
505 zoomed in 3 x 3 μm scan of particle edge. Line scan of (c) peptidoglycan particle at the Au coated
506 mica interface, showing a height of ~40 nm.

507
508
509
510
511
512
513
514
515
516
517



518
519
520
521
522
523
524
525
526
527
528
529
530
531
532
533
534
535 b
536
537
538
539
540
541
542
543
544
545
546
547
548
549
550
551
552
553 **Figure 5.** Raman spectra of (a) peptidoglycan in comparison with gold SERS substrate, *P.*
554 *aeruginosa* and MRSA. Pristine and wetted-then-dried SERS substrates reference spectra show no
555 correlation with peaks of interest. Normalized (b) spectra of peptidoglycan, *P. aeruginosa* and
556 MRSA showing a ~ 730 nm⁻¹ peak corresponding to glucose rings NAG and NAM molecules,
557 which reside in the peptidoglycan.



584
585 **Figure 6.** Topography and resistance 1 x 1 μm images of (a,b) bare gold and (c,d) peptidoglycan.
586 This peptidoglycan image is from the same peptidoglycan particle as in Figure 4. The average
587 resistance value for peptidoglycan particle on gold surface is 103 GΩ.